Chinese Journal of
POLYMER SCIENCE

RESEARCH ARTICLE

https://doi.org/10.1007/s10118-024-3124-6
Chinese J. Polym. Sci.

Reinforcement of High Impact Polystyrene by Aramid Nanoparticle Fillers Prepared *via* an *In situ* Bottom-up Approach

Xiang-Jun Gong, Zhi-Ping Zhao, Chang-Mei Sun*, Ying Zhang, Rong-Jun Qu*, and Ying Wang

School of Chemistry and Materials Science, Ludong University, Yantai 264025, China

Abstract In this work, aramid nanoparticles (ANPs) were prepared in dimethyl formamide (DMF) solution containing high impact polystyrene (HIPS) *via* a bottom-up approach. Transmission electron microscopy (TEM) images showed that the obtained ANPs were evenly distributed in the HIPS matrix without any agglomeration. Chemical composition of the ANPs, *i.e.*, poly(*p*-phenyl-*p*-phenylenediamine) (PPTA), was confirmed by Fourier transform infrared spectroscopy (FTIR), X-ray photoelectron spectroscopy (XPS) and X-ray diffractometer (XRD). The ANP/HIPS composites, obtained after ethanol precipitation, were added to neat HIPS as fillers to fabricate ANP/HIPS composite sheets. The surface roughness and the glass transition temperature (T_g) of the sheets were characterized by atomic force microscope (AFM) and differential scanning calorimetry (DSC), respectively. Compared with neat HIPS, the mechanical properties of the composite sheet were significantly improved, and the Young's modulus increased from 246.55 MPa to 2025.12 MPa, the tensile strength increased from 3.07 MPa to 29.76 MPa, and the toughness increased from 0.32 N/mm^2 to 3.92 N/mm^2, with an increase rate of 721%, 869% and 1125%, respectively. Moreover, the thermal stability of the composites improved with the increase in ANP content.

Keywords High impact polystyrene; PPTA nanoparticle; Reinforce; Mechanical property

Citation: Gong, X. J.; Zhao, Z. P.; Sun, C. M.; Zhang, Y.; Qu, R. J.; Wang, Y. Reinforcement of high impact polystyrene by aramid nanoparticle fillers prepared *via* an *in situ* bottom-up approach. *Chinese J. Polym. Sci.* https://doi.org/10.1007/s10118-024-3124-6

INTRODUCTION

High impact polystyrene (HIPS) is a type of modified polystyrene (PS) material by polybutadiene (PB).[1] Ease of processing, low cost, and non-toxicity of HIPS[2] render its wide uses in the electronics and medical industries and as a key military and construction material.[3] Although HIPS is a modified product of PS, the flame retardancy, toughness and strength of HIPS are still poor.[4]

Modification of the HIPS material to improve its properties has been the focus of many recent studies.[5] Modification efforts mainly fall into two categories—chemically functionalizing HIPS [6]and adding various composite fillers. Amongst the fillers, nanomaterials, such as SiO_2 nanoparticles,[7] $CaCO_3$ nanoparticles[8] and carbon nanotubes,[9] showed great promise in improving its flame retardancy and mechanical properties. For example, Chatterjee *et al*.[8] studied the rheology, thermal, mechanical and morphological properties of $CaCO_3$/HIPS nanocomposites. The experimental results showed that the rheology, thermal, mechanical and morphological properties of hybrid nano-$CaCO_3$/PS particles were enhanced in HIPS matrix. This filler approach, however, often encounters the issues of poor dispersion and ease of filler agglomeration, which would lead to abnormal growth of particles, formation of stress concentration points or defect points, and fast deterioration of polymer properties.[10,11]

Aramid fiber, also known as poly(*para*-phenylene terephthalamide) (PPTA), is a promising additive used to reinforce polymer matrices because of its excellent properties, such as high strength and modulus, non-flammability, *etc*.[12] However, the aromatic rings in the polymer backbone of PPTA macrofibers and the interchain hydrogen bonding between the $-NH_2$ and $-C=O$ functional groups result in rigidity and therefore smooth surface when used as a filler, which leads to poor distribution in the matrix and low interfacial bonding strength with the polymer.

Aramid nanofibers (ANFs), which was successfully prepared using a "top-down" method by Yang *et al*. in 2011,[13] compensate for some of the disadvantages of macro aramid fiber.[14] The large number of functional groups on the surface of ANFs enhances their interaction with the polymer matrix, compensating for the disadvantage of macroscopic fibers that have smooth surfaces and are difficult to bind other substances. ANFs combine some desirable characteristics of PPTA and nano materials, including good mechanical properties, high aspect ratio and surface area, which can improve reactivity and interfacial bonding strength with polymer.[15] For example, ANFs composited with poly(vinyl alcohol) (PVA) well,[16] and the resulting composites showed high tough-

* Corresponding authors, E-mail: sunchangmei0535@126.com (C.M.S.)
E-mail: rongjunqu@sohu.com (R.J.Q.)

Received January 9, 2024; Accepted March 11, 2024; Published online April 25, 2024

ness, tensile strength, and unexpected modified thermal stability. The interfacial adhesion of carbon fibers was found to be improved with the addition of ANFs.[17] At the same time, the addition of ANFs realized the toughening of the original masterbatch. Despite the interfacial compatibility issue addressed by ANFs, more problems remain such as ease of agglomeration, difficulty in dispersion, and long preparation time.[18]

Recently, our group successfully synthesized nano aramid in a PVC-containing solution *via* a "bottom-up" method.[19] Interestingly, the obtained nano aramid was observed to be spherical in shape, which made us realize that nano aramid can present in various forms besides the typical ANF line shape. The spherical nano aramid was named aramid nanoparticle (ANP) by us. It was subsequently discovered that the shapes of nano aramids varied with the polymer structures in the reaction solution. In a polystyrene-containing solution, nano aramids were obtained as nanorods and nanobundles.[20] All nano aramids with various shapes distributed uniformly and compatibly within the polymer matrices without undesirable agglomeration. Material performance including thermal stability and mechanical properties was greatly enhanced by the nano aramid fillers. In addition, the "bottom-up" approach takes only a few hours, whereas the "top-down" approach usually takes at least a week.

In this work, the synthesis of ANPs in HIPS systems using a "bottom-up" approach was reported. This simple and efficient synthesis method resulted in HIPS composites with good ANP dispersion. The maximum growth rates of Young's modulus, toughness and tensile strength of ANP/HIPS composite sheets reached 721%, 1125% and 869%, respectively, compared to neat HIPS. More interestingly, other properties of ANP/HIPS composites were also improved.

EXPERIMENTAL

Materials and Instruments

Materials

HIPS, *p*-phenylenediamine (PPD) and terephthaloyl chloride (TPC) were purchased from Shanghai Aladdin Biochemical Technology Co. Absolute ethanol was purchased from Sinopharm Chemical Reagent Company. The purity of these reagents ranged between 90% and 99%. Water used in this study was deionized (DI) water.

Instruments

Fourier transform infrared (FTIR) spectra were acquired by Thermo Nicolet iS50 FTIR spectrometer for 0.5×0.5 cm ANP/HIPS composite filler with a scanning wavenumber range of 400–4000 cm^{-1} and 64 scans with a resolution of 2 cm^{-1}. X-ray photoelectron spectroscopy (XPS) were acquired on a Thermo ESCALAB Xi XPS microprobe equipped with a K-AlK*α* X-ray source. Transmission electron microscopy (TEM) was carried out using a JEOL JEM-1230 microscope at 100 kV. The ANP/HIPS mixture solution diluted with solvent was dripped onto the copper grid and dried to prepare 2×2 mm sheets of ANP/HIPS composite filler for TEM sampling. Field emission scanning electron microscopy (FE-SEM) was carried out on the surface of ANP/HIPS composite sheets using a Hitachi SU8010 microscope. The morphology of the samples was observed by SEM at 2 kV, and then continued to observe the elemental composition of the surface of the same samples using energy dispersive X-ray spectroscopy (EDS). Atomic force microscopy (AFM) images were acquired by a Bruker ICON AFM with a SCANASYST-AIR tip. Composite fillers prepared from dried ANP/HIPS blend solutions were cut and pasted onto circular patches. Subsequently, the roughness of the upper surface of the composite filler was characterized in scanning mode. A Netzsch STA 409 PC/PG instrument was used to perform thermogravimetric analysis (TGA) and differential scanning calorimetry (DSC). For thermogravimetric analysis, the ANP/HIPS composite sheets were heated directly under nitrogen from 25 °C to 800 °C at a heating rate of 10 °C·min^{-1}. For DSC, 10×10 mm ANP/HIPS composite sheets were used to be heated in nitrogen at temperature intervals ranging from 25 °C to 100 °C at a heating rate of 20 °C·min^{-1}. The mechanical properties of the composite sheets were tested on an apparatus manufactured by Ingström (USA). The composite films were dried and cut into rectangles 50 mm long and 10 mm wide. The mechanical properties of each test sample were tested at a speed of 10 mm·min^{-1}.

Synthesis of ANP/HIPS Composite Filler

Table 1 shows the synthesis recipes of HIPS and ANP/HIPS with varied PPD and TPC contents. The ANP/HIPS composites are denoted as ANP/HIPS-*X*, where *X* is the level of PPD and TPC with 1 being the lowest and 3 having triple the amount of PPD and TPC in 1.

The preparation of ANP/HIPS can be found in the literature,[20] where the specific preparation process is shown below.

First, 7 g of HIPS was added to 70 mL of DMF and stirred at 60 °C for 3 h to obtain a clear colorless solution as matrix solution. In the second step, the matrix solution was divided into two parts, one for dissolving PPD and the other for dissolving TPC (as shown in Table 1). The TPC portion was added dropwise to the PPD portion in an ice bath, and then the polymerization reaction was carried out for 3 h at room temperature under dry nitrogen. Finally, the product solution (ANP/HIPS-*X*) was washed repeatedly with deionized water to pH neutrality to produce white pellets. The white pellets are dried at 50 °C to make the ANP/HIPS composite filler.

Table 1 Preparation recipes of ANP/HIPS composites.

Samples	DMF (mL)	HIPS (g)	PPD (g)	TPC (g)
HIPS	70	7	–	–
ANP/HIPS-1	70	7	0.1081	0.2030
ANP/HIPS-2	70	7	0.2162	0.4060
ANP/HIPS-3	70	7	0.3243	0.6090
ANP/HIPS-4	70	7	0.4324	0.8120
ANP/HIPS-5	70	7	0.5405	1.0150

https://doi.org/10.1007/s10118-024-3124-6

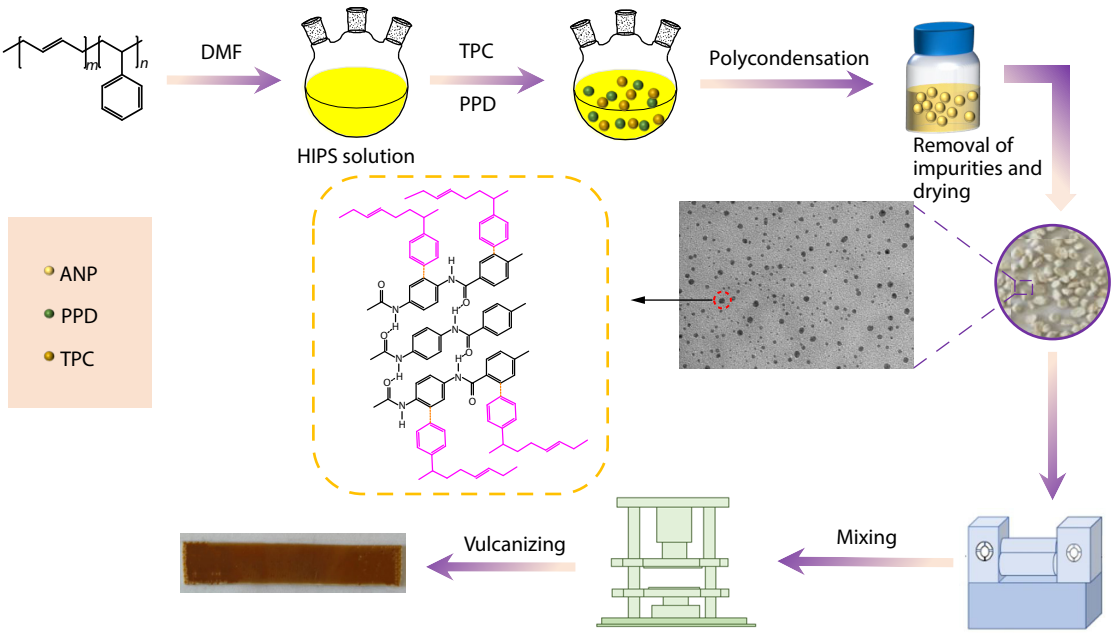

Fig. 1 Flowchart of the experimental preparation of ANP/HIPS composite sheet.

Preparation of ANP/HIPS Composite Sheet

ANP/HIPS composite fillers (4 g) and HIPS masterbatch (28 g) were mixed together and thoroughly blended at 150 °C in a two-roll mixer. The well-mixed samples were cut into small pieces and put into a plate vulcanizer for hot pressing at 165 °C for 20 min and cold pressing at room temperature for 10 min, both at a pressure of 10 MPa, in a 6 cm × 8 cm × 1 cm mold. The final product of ANP/HIPS composite films were thus obtained. The specific synthesis process can be seen in Fig. 1.

RESULTS AND DISCUSSION

FTIR Analysis of ANP/HIPS Composite Filler

The FTIR spectra of neat HIPS and ANP/HIPS-1 to ANP/HIPS-5 nanocomposites are shown in Fig. 2. The characteristic bands of PPTA at 3328, 1540 and 1317 cm^{-1} are present in the composite samples, indicating the formation of PPTA. Their band heights also increase with the starting PPD and TPC monomer contents as expected.[21]

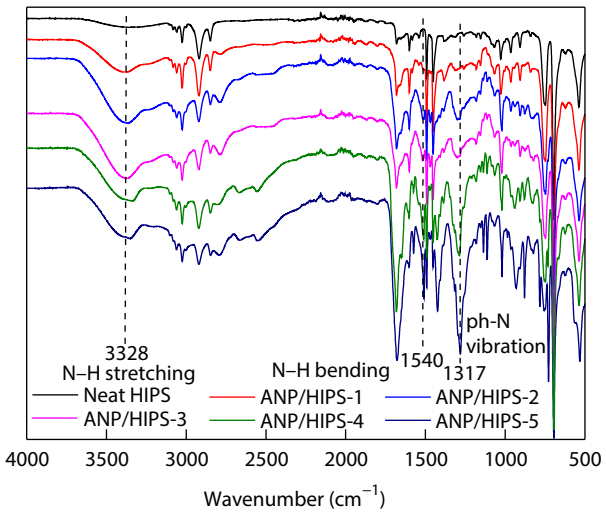

Fig. 2 FTIR spectra of neat HIPS and ANP/HIPS-*X* samples

XPS Analysis of ANP/HIPS Composite Filler

Fig. 3(a) compares the XPS spectra of neat HIPS and ANP/HIPS-*X* composites. An additional N 1s peak is present in the composites. The N 1s peak of ANP/HIPS-5 was fitted to the split peaks using CasaXPS, as shown in Fig. 3(c). The characteristic peak of the amide bond (N—C=O) in ANP appears at 399.7 eV. As shown in Fig. 3(b), the C 1s peak of the same sample was also fitted to the split peaks at 284.2, 284.6 and 286.2 eV, corresponding to the presence of O=C—N, C—C, C=C and C—N bonds, respectively.[22] The expected chemical bonds of PPTA were therefore confirmed by XPS.

FTIR and XPS results show the formation of PPTA in the HIPS matrix. The ANP composed of PPTA molecules can act as a nanofiller for HIPS and interact with the polymer matrix through the abundant functional groups on its surface, through which the binding ability with the polymer matrix can be enhanced and the mechanical properties of HIPS can be strengthened.

Micromorphological Analysis of ANP/HIPS Composite Filler

As shown in the TEM images of the ANP/HIPS-*X* nanocomposites in Fig. 4, the ANPs in the composites are spherical and well distributed with no significant particle aggregation. This may be due to the steric hindrance of long chains of HIPS matrix to the chain growth of the PPTA from the monomers PPD and TPC. As a result, only short chains of PPTA intertwine in the solvent DMF to form spheres. The well dispersed ANPs lead to improved mechanical properties of HIPS. Another interesting observation is that the average particle size increases with the ANP content. This may be due to the increase in solution viscosity with the monomer content, and longer PPTA molecular tend to be formed. As a result, larger ANPs can be obtained. The formation of spheres may be attributed to high solution viscosity, slow

https://doi.org/10.1007/s10118-024-3124-6

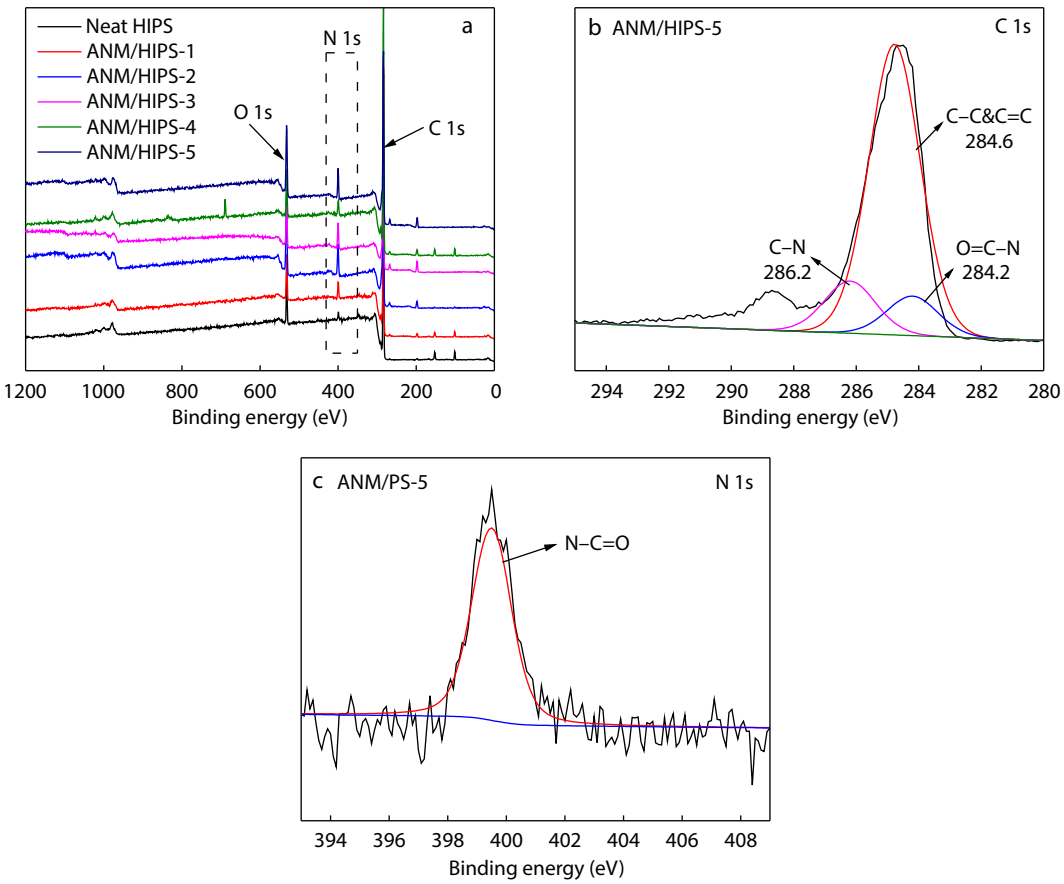

Fig. 3 (a) Overlaid XPS spectra of samples; (b) C 1s spectra of ANP/HIPS-5; (c) N 1s spectra of ANP/HIPS-5.

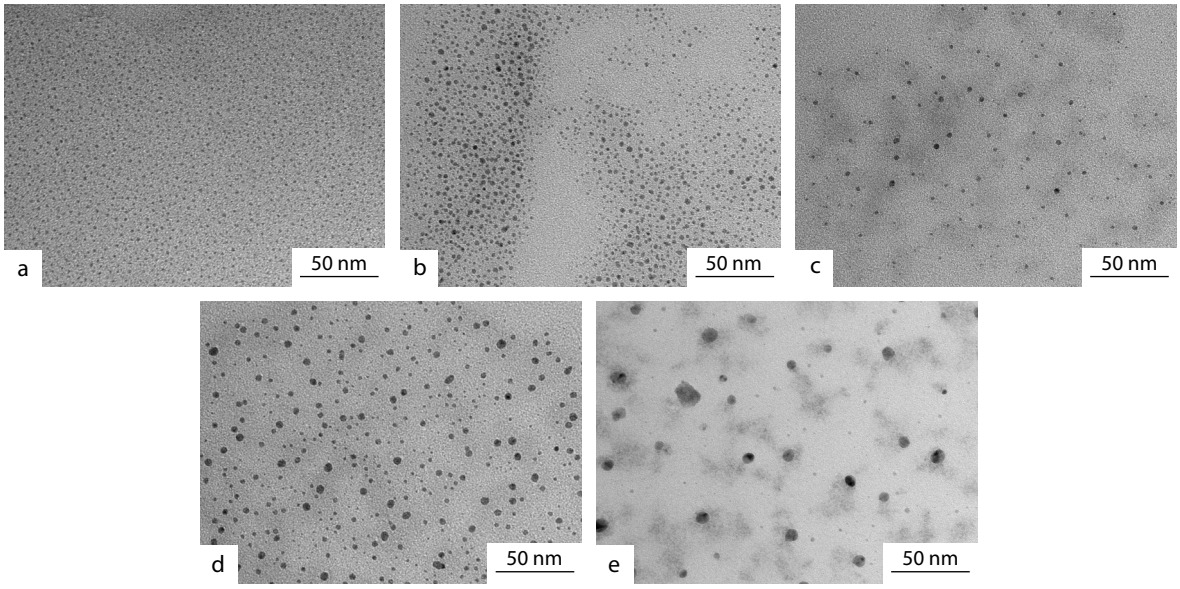

Fig. 4 TEM images of ANP/HIPS nanocomposites: (a) ANP/HIPS-1, (b) ANP/HIPS-2, (c) ANP/HIPS-3, (d) ANP/HIPS-4, (e) ANP/HIPS-5.

movement of matrix and entanglement of PPTA chains.[23,24]

Fig. 5 shows polarized light microscopy images of ANP synthesized *in situ* in HIPS systems with different monomer PPD/TPC contents. Figs. 5(a)–5(c) show the samples with lower monomer contents, the ANP crystals (black dots) exist almost entirely as well-dispersed mono-spherical crystals. At higher monomer contents as shown in Figs. 5(d)–5(e), crystal aggregation occurs at 30 °C due to an increase in the number of crystals per unit volume.[20]

XRD Analysis of ANP/HIPS Composite Sheet

XRD patterns of ANP/HIPS-1 to ANP/HIPS-5 samples in Fig. 6

https://doi.org/10.1007/s10118-024-3124-6

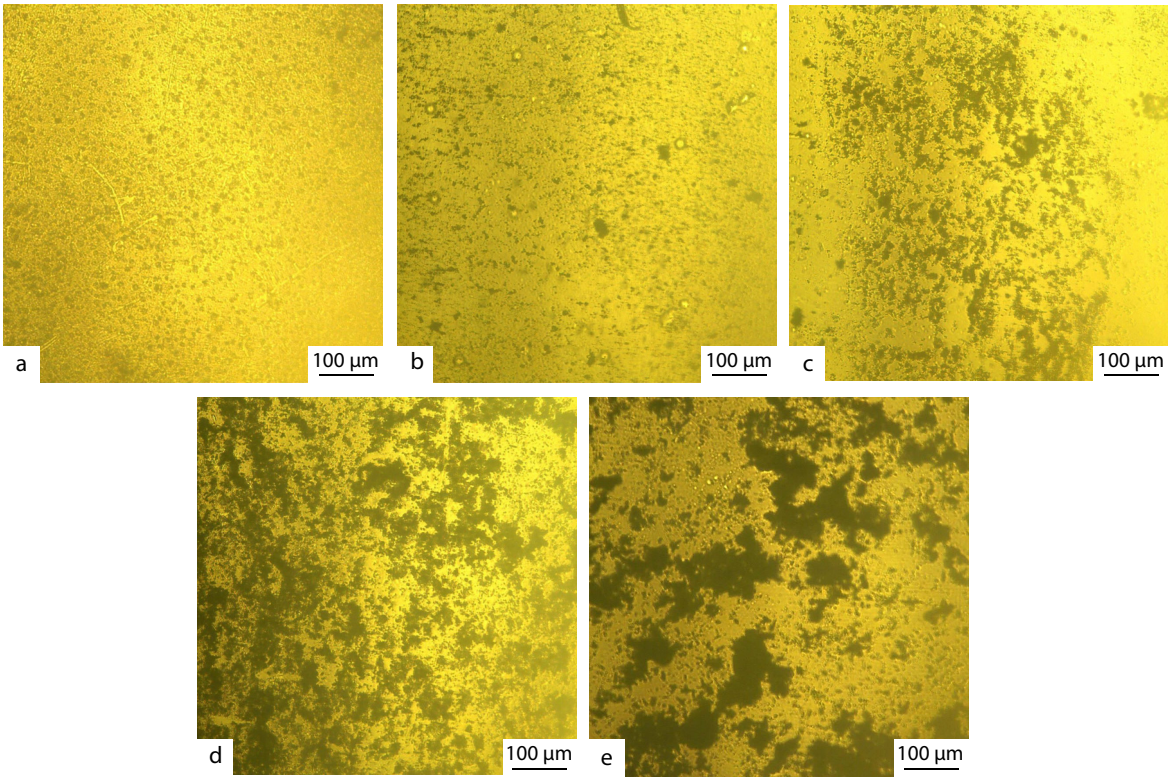

Fig. 5 Polarizing microscope images of (a) ANP/HIPS-1, (b) ANP/HIPS-2, (c) ANP/HIPS-3, (d) ANP/HIPS-4 and (e) ANP/HIPS-5.

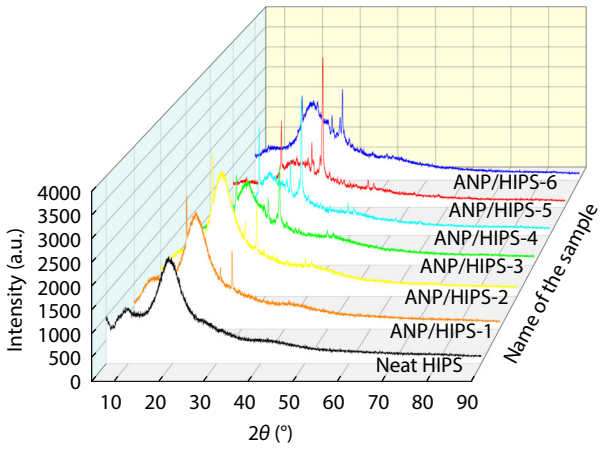

Fig. 6 XRD patterns of neat HIPS and ANP/HIPS samples at 25°C

show peaks at similar positions to those of the Kevlar (PPTA) characteristic peaks at 2θ angles of 18°, 25° and 29°, which correspond to reflections at positions (110), (200) and (004), respectively. Based on the three lattice planes corresponding to the above three diffraction peaks, the crystallinity (X_c) can be calculated by Eq. (1) and the results are listed in Table 2.

$$X_c = A_s/A_g \times 100\% \quad (1)$$

where A_s is area from integration of the strongest diffraction peaks, A_g is area from standard substance integration.

The diffraction peak positions of the ANP/HIPS composite filler are similar to those of the peaks of the neat PPTA, which confirms the formation of PPTA in the HIPS matrix.[16,25] Similarly, the peak intensities also increase with the starting PPD and TPC monomer contents. However, the ANP/HIPS-6 sample had a change in the amount of ANP produced due to excessive monomer additions, an increase in the viscosity of the solution, and a slow movement of the monomers. This could be due to the combined effect of covalent bonding between the amide bond and the benzene ring as well as the π-π conjugation effect, inducing the growth of the crystals in the direction of the a-axis, which results in the intensity enhancement of the diffraction peaks.[26]

Table 2 Crystallinity of neat HIPS and ANP/HIPS-*X*.

Samples	A_s	A_g	X_c (%)
ANP/HIPS-1	571.82	152.66	26.65
ANP/HIPS-2	239.94	899.86	26.66
ANP/HIPS-3	356.68	1131.57	31.52
ANP/HIPS-4	607.36	1373.80	44.21
ANP/HIPS-5	850.00	1550.95	54.81
ANP/HIPS-6	273.09	989.17	27.61

The formation of PPTA material in the ANP/HIPS-*X* composites *via* direct "*in situ* polymerization" of PPD and TPC monomers was therefore confirmed by FTIR, XRD analysis and XPS.

SEM-EDS Analysis of ANP/HIPS Composite Sheet

SEM images of upper surfaces of neat HIPS and ANP/HIPS-*X* nanocomposite samples are shown in Fig. 7. Neat HIPS has a flat surface (Fig. 7a), while the surface roughness of the composite increases with the monomer content (Figs. 7b–7f). The EDS images of ANP/HIPS-5 are shown in Fig. 8. The N (in green) and O (in yellow), both unique to PPTA, are well dispersed in the images without forming large aggregates. This indicates that PPTA is well dispersed in the HIPS matrix and can be well compatible with HIPS.[27,28]

https://doi.org/10.1007/s10118-024-3124-6

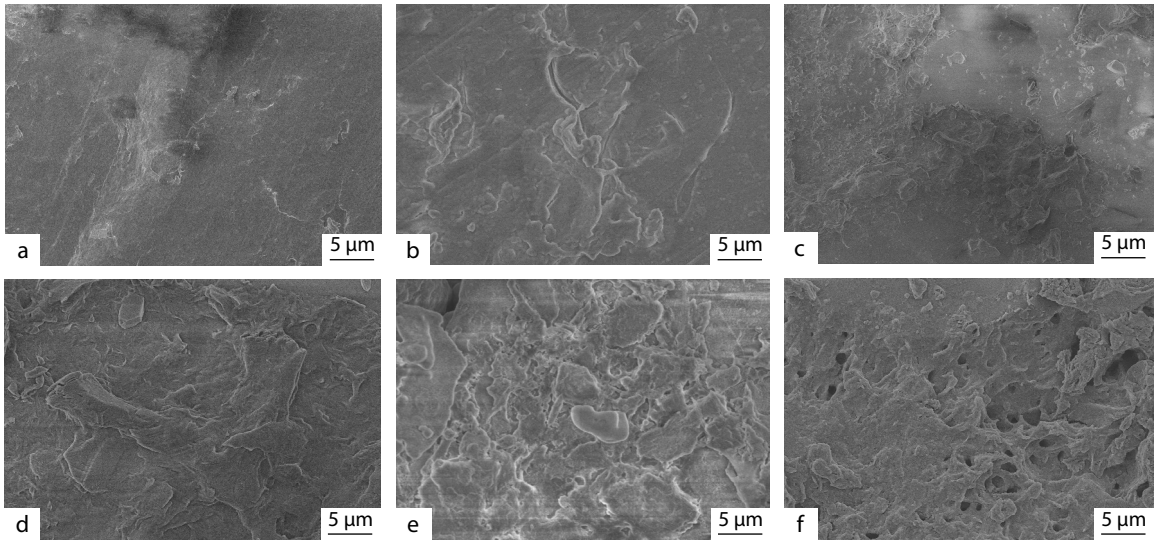

Fig. 7 SEM images of top surfaces of (a) HIPS and (b–f) ANP/HIPS-*X*: (b) ANP/HIPS-1, (c) ANP/HIPS-2, (d) ANP/HIPS-3, (e) ANP/HIPS-4, (f) ANP/HIPS-5.

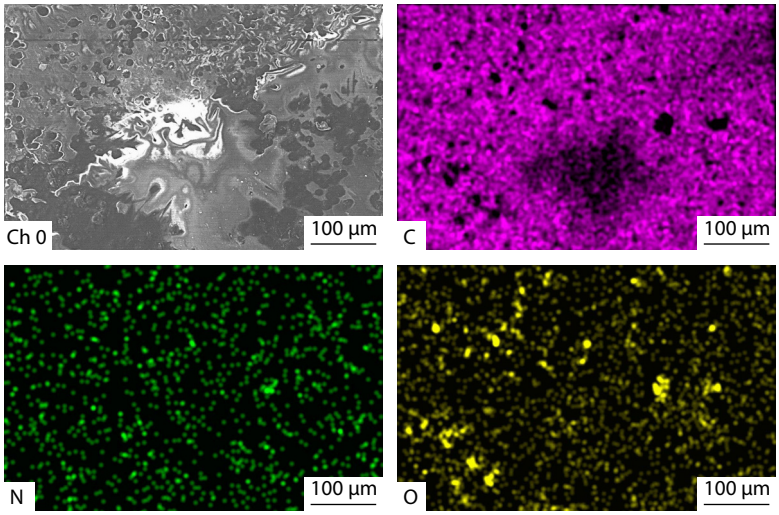

Fig. 8 EDS images of ANP/HIPS-5.

AFM Analysis of ANP/HIPS Composite Sheet

Fig. 9 shows the AFM results of HIPS and ANP/HIPS-*X* composite films and the roughness values are listed in Table 3. The average roughness (R_a) is 1.06 nm for neat HIPS (1.06 nm) and ranges from 1.58 nm to 4.72 nm for ANP/HIPS-*X* composites. A positive correlation can be observed between R_a of nanocomposites and the ANP content. This phenomenon may occur as the monomer PPD/TPC content increases, the dense layer formed during the process of blending and vulcanization with HIPS becomes thinner, resulting in increased roughness. Moreover, the compatibility between the solvent DMF and water is poor, which leads to increased surface roughness of ANP/HIPS-*X*. A third contributing factor may be temperature, which leads to thermodynamic instability and the tendency of ANP nanoparticles to copolymerize during the process of blending and vulcanization with the masterbatch, increasing roughness.[29]

Thermal Stability Analysis of ANP/HIPS Composite Sheet

The DSC curves labelled with the glass transition temperature (T_g) of the samples are shown in Fig. 10. All samples only exhibit one phase transition step (one peak), suggesting that the ANPs are well dispersed. For materials having multiple phases, multiple phase transitions may occur.

This confirms the observations in the microscopic images discussed previously. The ANP/HIPS-*X* nanocomposites see a positive correlation between T_g and the ANP content, that is, the value of T_g increased from 64.76 °C to 101.04 °C with increasing ANP content. As ANPs can effectively impede the movement of the polymer chain segments of HIPS, higher temperature is required during phase transition to free up those chain segments for composites containing higher content of ANPs. The higher T_g values of the composites versus pure HIPS also indicate improved thermal stability of the composites.[30]

The TGA curves of composites are shown in Fig. 11. The weight loss between 300–350 °C is attributed to the thermal decomposition of the HIPS matrix material and the formation of its volatile degradation products. A second weight loss in

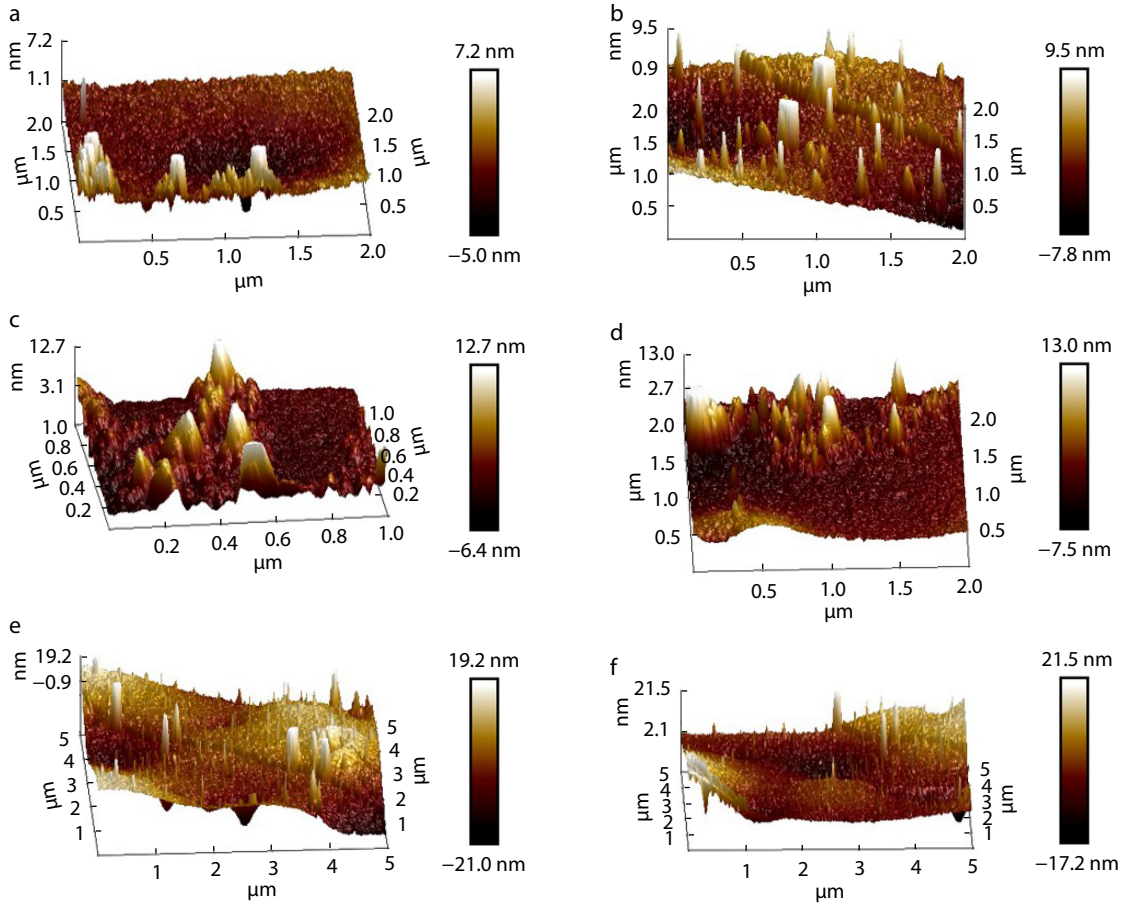

Fig. 9 AFM results of (a) HIPS and (b–f) ANP/HIPS-*X*: (b) ANP/HIPS-1, (c) ANP/HIPS-2, (d) ANP/HIPS-3, (e) ANP/HIPS-4, (f) ANP/HIPS-5.

Table 3 Roughness values of samples.

Samples	Roughness		
	R_a (nm)	R_q (nm)	R_{max} (nm)
Neat HIPS	1.06	1.53	23.7
ANP/HIPS-1	1.77	2.57	41.7
ANP/HIPS-2	1.58	2.32	22.4
ANP/HIPS-3	1.74	2.59	31.4
ANP/HIPS-4	4.72	6.11	109
ANP/HIPS-5	4.15	5.52	67.9

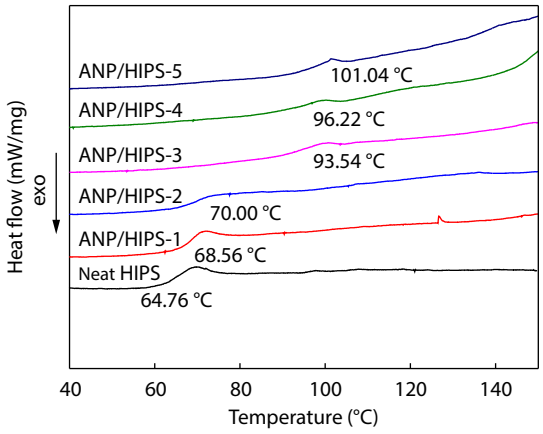

Fig. 10 DSC curves of neat HIPS and ANP/HIPS-1 to ANP/HIPS-5.

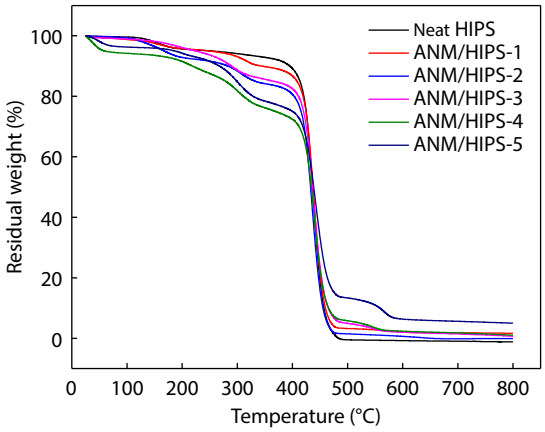

Fig. 11 TGA curves of neat HIPS and ANP/HIPS-*X*.

the 500–600 °C region is due to the thermal decomposition of the ANPs. As shown in the literature,[31] more monomer content in the HIPS matrix has no great influence on the thermal stability performance of PPTA.[32]

Analysis of Mechanical Properties of ANP/HIPS Sample Sheet

The mechanical stress-strain curves for neat HIPS and ANP/HIPS-*X* nanocomposites are shown in Fig. 12. The values of tensile strength, toughness, and Young's modulus obtained from a uni-

https://doi.org/10.1007/s10118-024-3124-6

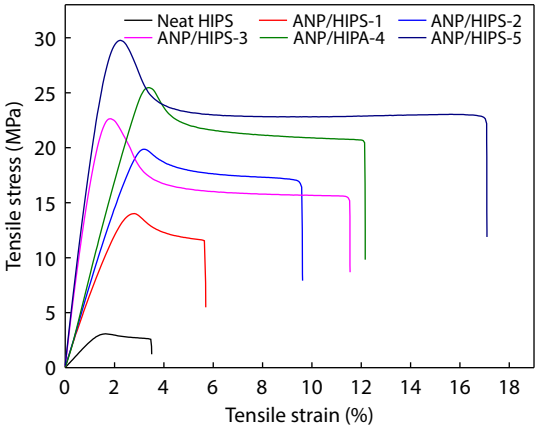

Fig. 12 Stress-strain diagrams of neat HIPS and ANP/HIPS-*X*.

Table 4 Mechanical properties of samples.

Sample	Young's modulus (MPa)	Toughness (N/mm^2)	Tensile stress (MPa)
HIPS	246.55	0.32	3.07
ANP/HIPS-1	682.64 (176%)	0.59 (84%)	14.01 (356%)
ANP/HIPS-2	771.74 (212%)	1.51 (371%)	19.86 (546%)
ANP/HIPS-3	1908.17 (673%)	1.87 (484%)	22.63 (637%)
ANP/HIPS-4	900.72 (265%)	2.36 (637%)	25.41 (727%)
ANP/HIPS-5	2025.12 (721%)	3.92 (1125%)	29.76 (869%)

versal material testing machine are listed in Table 4 with the percentage increase over the neat HIPS in parentheses. The ANP/HIPS-*X* nanocomposites significantly improved mechanical properties against neat HIPS as shown by stress-strain curves. The degrees of improvement are also positively correlated with the ANP content. ANP/HIPS-5 has the most significant improvement, showing a 721% increase in the Young's modulus, an 869% increase in tensile strength, and above all a 1125% increase in toughness from 0.32 N/mm^2 to 3.92 N/mm^2. The toughness of the composite material, as imparted by the ANP fillers, may derive from the macroscopic PPTA. As shown previously that the molecular weight of ANP increases with the monomer content, the strengthening effect of HIPS is more significant, potentially enabling practical industrial production of HIPS materials.[33,34]

Table 5 Comparison of tensile stress of ANP/HIPS composites with other modifiers.

Modifiers	Tensile stress (MPa)	References
Multiwalled carbon nanotubes (MWNT)	25.5	[35]
Aluminum nitride	15.2	[36]
Coconut fiber	24.51	[37]
Rubber toughened glass fibre	13	[2]
Recycled polypropylene (R-PP)	22.91	[38]
ANP	29.76	This study

Table 5 shows the comparison of tensile stresses of HIPS composites in other studies and it can be clearly seen that the tensile stresses of ANP/HIPS composites in the present study have improved very significantly. This indicates that the mechanical properties of HIPS can be effectively improved by the ANP prepared by the "bottom-up" *in situ* polymerization method. Moreover, this method is simple, safe and efficient.

The SEM photos of the fracture surfaces of composites after stretching are presented in Fig. 13. The fracture surface of HIPS (Fig. 12a) is clearly flatter and smoother, confirming the observation in the AFM image. With the introduction of ANPs, the fracture starts to appear rough to different degrees, showing a "drawn" form. With the increase of ANP content, the composites show a gradual trend from brittle fracture to ductile fracture, suggesting improved toughness of the composite materials. ANPs, as a rigid rod-like molecule, are thermodynamically incompatible with HIPS, prompting their uniform dispersion in the ANP/HIPS system. The composites have limited compatibility at high temperatures during mixing with the masterbatch. They do not segregate in the matrix to form suspensions, but exist in a form similar to uniformly dispersed microspheres with good stability.[39]

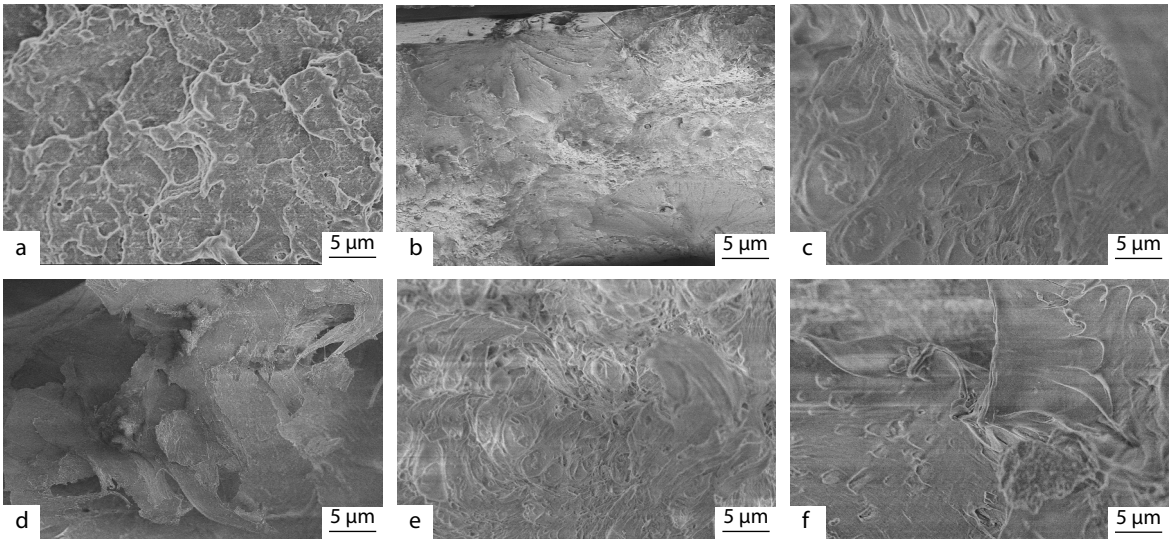

Fig. 13 SEM images of cross sections of (a) HIPS, (b) ANP/HIPS-1, (c) ANP/HIPS-2, (d) ANP/HIPS-3, (e) ANP/HIPS-4 and (f) ANP/HIPS-5.

https://doi.org/10.1007/s10118-024-3124-6

CONCLUSIONS

In this work, ANP was successfully synthesized in a HIPS-containing solution by *in situ* "bottom-up" polymerization, producing an ANP/HIPS composite filler. A composite sheet was fabricated by blending the ANP/HIPS filler with neat HIPS. As confirmed by a series of characterization methods, the filler-enhanced composite sheets showed a striking improvement in toughness and other mechanical properties as well. The toughness increase rate of ANP/HIPS composites can reach up to 1125% and the increase rate of Young's modulus is 721%. ANP is a new nanofiller material especially suited for toughening HIPS. This finding also provides a promising new direction for the subsequent industrial production of HIPS.

Conflict of Interests

The authors declare no interest conflict.

Data Availability Statement

The data that support the findings of this study are available on request from the corresponding author upon reasonable request. The authors' contact information: sunchangmei0535@126.com (C.M.S.), rongjunqu@sohu.com (R.J.Q.).

ACKNOWLEDGMENTS

This work was financially supported by Innovation Project for graduate students of Ludong University (No. IPGS2024-058) and the National Natural Science Foundation of China (Nos. 52073135, 51673089 and 51903114).

REFERENCES

1 Arif, S.; Kautek, W. Pulse laser machining and particulate separation from high impact polystyrene. *Appl. Surf. Sci.* **2014**, *288*, 9−14.
2 Alsewailem, F. D.; Al-ameri, A. M. Rubber toughened glass fibre reinforced high impact polystyrene. *Mater. Sci. Technol.* **2023**, *39*, 1973−1976.
3 Kong, Y. F.; Li, Y. C.; Hu, G. S.; Cao, N.; Ling, Y. Q.; Pan, D.; Shao, Q.; Guo, Z. H. Effects of polystyrene-*b*-poly(ethylene/propylene)-*b*-polystyrene compatibilizer on the recycled polypropylene and recycled high-impact polystyrene blends. *Polym. Adv. Technol.* **2018**, *29*, 2344−2351.
4 Jelcic, Z.; Ranogajec, F. Radiation modified high impact polystyrene. *Radiat. Phys. Chem.* **2012**, *81*, 1366−1369.
5 Katancic, Z.; Travas-Sejdic, J.; Hrnjak-Murgic, Z. Flammability and thermal properties of zeolite-filled high-impact polystyrene composites. *Polym. Plast. Technol. Eng.* **2014**, *53*, 1487−1493.
6 Mohan, A. J.; Sekhar, V. C.; Bhaskar, T.; Nampoothiri, K. M. Microbial assisted high impact polystyrene (HIPS) degradation. *Bioresour. Technol.* **2016**, *213*, 204−207.
7 Valeros, A.; Panganiban, A.; Millare, J. Fabrication and characterization of nanozeolite-modified high impact polystyrene (HIPS) membranes for nanofiltration. *Key Eng. Mater.* **2022**, *931*, 93−98.
8 Chatterjee, A.; Mishra, S. Nano-calcium carbonate ($CaCO_3$)/Polystyrene (PS) core-shell nanoparticle: it's effect on physical and mechanical properties of high impact polystyrene (HIPS). *J. Polym. Res.* **2013**, *20*, 12.
9 Zhou, Y. M.; Wang, L. L.; Li, X. P.; Wang, X. F.; Jiang, H. T. Effect of nano-carbon addition on color performance of polystyrene superstructure film. *J. Ceram. Process. Res.* **2018**, *19*, 479−482.
10 Kostas, V.; Baikousi, M.; Barkoula, N. M.; Giannakas, A.; Kouloumpis, A.; Avgeropoulos, A.; Gournis, D.; Karakassides, M. A. Synthesis, characterization and mechanical properties of nanocomposites based on novel carbon nanowires and polystyrene. *Appl. Sci.* **2020**, *10*, 5737.
11 Yin, J.; Retsch, M.; Thomas, E. L.; Boyce, M. C. Collective mechanical behavior of multilayer colloidal arrays of hollow nanoparticles. *Langmuir* **2012**, *28*, 5580−5588.
12 Dong, C.; Fu, R.; Sun, C.; Qu, R.; Ji, C.; Niu, Y.; Zhang, Y. Comparison studies of adsorption properties for copper ions in fuel ethanol and aqueous solution using silica-gel functionalized with 3-amino-1,2-propanediol. *Fuel* **2018**, *226*, 331−337.
13 Yang, M.; Cao, K. Q.; Sui, L.; Qi, Y.; Zhu, J.; Waas, A.; Arruda, E. M.; Kieffer, J.; Thouless, M. D.; Kotov, N. A. Dispersions of aramid nanofibers: a new nanoscale building block. *ACS Nano* **2011**, *5*, 6945−6954.
14 Dewilde, S.; Vander Hoogerstraete, T.; Dehaen, W.; Binnemans, K. Synthesis of poly-*p*-phenylene terephthalamide (PPTA) in ionic liquids. *ACS Sustainable Chem. Eng.* **2018**, *6*, 1362−1369.
15 Sun, Z.; Zhou, Y.; Li, W.; Chen, S.; You, S.; Ma, J. Preparation of silver-plated para-aramid fiber by employing low-temperature oxygen plasma treatment and dopamine functionalization. *Coatings* **2019**, *9*, 17.
16 Guan, Y.; Li, W.; Zhang, Y.; Shi, Z.; Tan, J.; Wang, F.; Wang, Y. Aramid nanofibers and poly(vinyl alcohol) nanocomposites for ideal combination of strength and toughness *via* hydrogen bonding interactions. *Compos. Sci. Technol.* **2017**, *144*, 193−201.
17 Lee, J. U.; Park, B.; Kim, B. S.; Bae, D. R.; Lee, W. Electrophoretic deposition of aramid nanofibers on carbon fibers for highly enhanced interfacial adhesion at low content. *Compos. Part A: Appl. Sci. Manuf.* **2016**, *84*, 482−489.
18 Yang, B.; Zhang, M. Y.; Lu, Z. Q.; Luo, J. J.; Song, S. X.; Zhang, Q. Y. From poly(*p*-phenylene terephthalamide) broken paper: high-performance aramid nanofibers and their application in electrical insulating nanomaterials with enhanced properties. *ACS Sustainable Chem. Eng.* **2018**, *6*, 8954−8963.
19 Peng, G.; Yaoqin, W.; Changmei, S.; Chunnuan, J.; Ying, Z.; Rongjun, Q.; Ying, W. Preparation and properties of PVC-based ultrafiltration membrane reinforced by *in-situ* synthesized p-aramid nanoparticles. *J. Membr. Sci.* **2022**, *642*, 12.
20 Wu, Y.; Zhao, Z.; Sun, C.; Ji, C.; Zhang, Y.; Qu, R.; Wang, Y. *In-situ* synthesis of PPTA nanomaterials in PS matrix and their enhanced performances in PS-based nanocomposite. *European Polymer Journal* **2022,** *179*, 11.
21 Zhu, J.; Yang, M.; Emre, A.; Bahng, J. H.; Xu, L.; Yeom, J.; Yeom, B.; Kim, Y.; Johnson, K.; Green, P.; Kotov, N. A. Branched aramid nanofibers. *Angew. Chem. Int. Ed.* **2017**, *56*, 11744−11748.
22 Lin, J. J.; Bang, S. H.; Malakooti, M. H.; Sodano, H. A. Isolation of aramid nanofibers for high strength and toughness polymer nanocomposites. *ACS Appl. Mater. Interfaces* **2017**, *9*, 11167−11175.
23 Kong, X.; Geng, X.; Geng, S.; Qu, R.; Zhang, Y.; Sun, C.; Wang, J.; Wang, Y.; Ji, C. Antibacterial para-aramid fiber loaded with *in situ* generated silver nanoparticles. *Surfaces and Interfaces* **2022**, *30*, 10.
24 Chae, H. G.; Kumar, S. Rigid-rod polymeric fibers. *J. Appl. Polym. Sci.* **2006**, *100*, 791−802.
25 Teng, C.; Li, H.; Liu, J.; Gu, H.; Kong, H.; Yu, M. Effect of high molecular weight PPTA on liquid crystalline phase and spinning

process of aramid fibers. *Polymers* **2020**, *12*, 1206.
26 Geng, X.; Kong, X.; Geng, S.; Qu, R.; Wang, J.; Zhang, Y.; Sun, C.; Ji, C. Conductive aramid fibers from electroless silver plating of crosslinked HPAMAM-modified PPTA: preparation and properties. *ACS Omega* **2022**, *7*, 17014−17023.
27 Saxena, A.; Prabhakaran, P. V.; Rao, V. L.; Ninan, K. N. synthesis and characterization of polyamides and poly(amide-imide)s derived from 2,2-bis(4-aminophenoxy) benzonitrile. *Eur. Polym. J.* **2003**, *39, 401–405* **2002,** *39*, 401-405.
28 Li, T.; Li, L.; Xu, Q.; Wang, Y.; Li, Y. Synthesis and mechanical properties of high impact polystyrene within situbulk polymerization toughened by one-pot Nd-based styrene-isoprene-butadiene terpolymer rubber. *J. Appl. Polym. Sci.* **2016**, *133*, 8.
29 Shi, Q.; Ni, L.; Zhang, Y. F.; Feng, X. S.; Chang, Q. H.; Meng, J. Q. Poly(*p*-phenylene terephthamide) embedded in a polysulfone as the substrate for improving compaction resistance and adhesion of a thin film composite polyamide membrane. *J. Mater. Chem. A* **2017**, *5*, 13610−13624.
30 Chen, X.; Wang, W.; Li, S.; Jiao, C. Fire safety improvement of para-aramid fiber in thermoplastic polyurethane elastomer. *J. Hazard. Mater.* **2017**, *324*, 789−796.
31 Fan, J. C.; Wang, J. L.; Shi, Z. X.; Yu, S.; Yin, J. Kevlar nanofiber-functionalized multiwalled carbon nanotubes for polymer reinforcement. *Mater. Chem. Phys.* **2013**, *141*, 861−868.
32 Zhao, Z.; Gong, X.; Sun, C.; Zhang, Y.; Qu, R.; Wang, Y. Preparation and properties of SBR/PPTA nanocomposite *via in-situ* interfacial polycondensation. *J. Appl. Polym. Sci.* **2023**, *140*, 14.
33 Peng, G.; Yaoqin, W.; Congcong, D.; Changmei, S.; Rongjun, Q.; Chunnuan, J.; Ying, Z.; Ying, W. Allyl and benzyl modified aramid nanofibers as an enhancement in polystyrene-based composites. *Front. Chem.* **2020**, *8*, 586763.
34 Zhang, Y.; Lu, H.; Zhang, M.; Hou, Z.; Li, S.; Wang, H.; Wu, X. E.; Zhang, Y. *In situ* mineralizing spinning of strong and tough silk fibers for optical waveguides. *ACS Nano* **2023**, *17*, 5905−5912.
35 Li, J. Effect of multiwalled carbon nanotubes (MWNT) on the properties of high impact polystyrene (HIPS). *J. Nanomater.* **2018**, *2018*, 1−5.
36 Thuong, N. T.; Lam, N. B.; Son, P. A.; Chien, N. B.; Linh, N. P. D.; Nam, C. T. H.; Vu, N. A.; Caggiano, A. Preparation and characterization of thermally conductive high impact polystyrene/AlN composite. *Int. J. Polym. Sci.* **2024**, *2024*, 1−9.
37 Carvalho, K. C. C.; Mulinari, D. R.; Voorwald, H. J. C.; Cioffi, M. O. H. Chemical modification effect on the mechanical properties of HIPS/coconut fiber composites. *BioResources* **2010**, *5*, 1143−1155.
38 Kong, Y.; Li, Y.; Hu, G.; Lin, J.; Pan, D.; Dong, D.; Wujick, E.; Shao, Q.; Wu, M.; Zhao, J.; Guo, Z. Preparation of polystyrene-*b*-poly(ethylene/propylene)-*b*-polystyrene grafted glycidyl methacrylate and its compatibility with recycled polypropylene/recycled high impact polystyrene blends. *Polymer* **2018**, *145*, 232−241.
39 Ma, Y. X.; Shi, F. M.; Ma, J.; Wu, M. N.; Zhang, J.; Gao, C. J. Effect of PEG additive on the morphology and performance of polysulfone ultrafiltration membranes. *Desalination* **2011**, *272*, 51−58.

https://doi.org/10.1007/s10118-024-3124-6